View metadata, citation and similar papers at core.ac.uk

brought to you by CORE

provided by Lancaster E-Prints

Physics Letters B 752 (2016) 18–26

Contents lists available at ScienceDirect

Physics Letters B

www.elsevier.com/locate/physletb

Precise measurement of the top quark mass in dilepton decays using optimized neutrino weighting

D0 Collaboration

V.M. Abazov [af], B. Abbott [bp], B.S. Acharya [z], M. Adams [au], T. Adams [as], J.P. Agnew [ap], G.D. Alexeev [af], G. Alkhazov [aj], A. Alton [be,1], A. Askew [as], S. Atkins [bc], K. Augsten [g], C. Avila [e], F. Badaud [j], L. Bagby [at], B. Baldin [at], D.V. Bandurin [bv], S. Banerjee [z], E. Barberis [bd], P. Baringer [bb], J.F. Bartlett [at], U. Bassler [o], V. Bazterra [au], A. Bean [bb], M. Begalli [b], L. Bellantoni [at], S.B. Beri [x], G. Bernardi [n], R. Bernhard [t], I. Bertram [an], M. Besançon [o], R. Beuselinck [ao], P.C. Bhat [at], S. Bhatia [bg], V. Bhatnagar [x], G. Blazey [av], S. Blessing [as], K. Bloom [bh], A. Boehnlein [at], D. Boline [bm], E.E. Boos [ah], G. Borissov [an], M. Borysova [am,12], A. Brandt [bs], O. Brandt [u], R. Brock [bf], A. Bross [at], D. Brown [n], X.B. Bu [at], M. Buehler [at], V. Buescher [v], V. Bunichev [ah], S. Burdin [an,2], C.P. Buszello [al], E. Camacho-Pérez [ac], B.C.K. Casey [at], H. Castilla-Valdez [ac], S. Caughron [bf], S. Chakrabarti [bm], K.M. Chan [az], A. Chandra [bu], E. Chapon [o], G. Chen [bb], S.W. Cho [ab], S. Choi [ab], B. Choudhary [y], S. Cihangir [at], D. Claes [bh], J. Clutter [bb], M. Cooke [at,11], W.E. Cooper [at], M. Corcoran [bu], F. Couderc [o], M.-C. Cousinou [l], J. Cuth [v], D. Cutts [br], A. Das [bt], G. Davies [ao], S.J. de Jong [ad,ae], E. De La Cruz-Burelo [ac], F. Déliot [o], R. Demina [bl], D. Denisov [at], S.P. Denisov [ai], S. Desai [at], C. Deterre [ap,3], K. DeVaughan [bh], H.T. Diehl [at], M. Diesburg [at], P.F. Ding [ap], A. Dominguez [bh], A. Dubey [y], L.V. Dudko [ah], A. Duperrin [l], S. Dutt [x], M. Eads [av], D. Edmunds [bf], J. Ellison [ar], V.D. Elvira [at], Y. Enari [n], H. Evans [ax], A. Evdokimov [au], V.N. Evdokimov [ai], A. Fauré [o], L. Feng [av], T. Ferbel [bl], F. Fiedler [v], F. Filthaut [ad,ae], W. Fisher [bf], H.E. Fisk [at], M. Fortner [av], H. Fox [an], S. Fuess [at], P.H. Garbincius [at], A. Garcia-Bellido [bl], J.A. García-González [ac], V. Gavrilov [ag], W. Geng [l,bf], C.E. Gerber [au], Y. Gershtein [bi], G. Ginther [at,bl], O. Gogota [am], G. Golovanov [af], P.D. Grannis [bm], S. Greder [p], H. Greenlee [at], G. Grenier [q,r], Ph. Gris [j], J.-F. Grivaz [m], A. Grohsjean [o,3], S. Grünendahl [at], M.W. Grünewald [aa], T. Guillemin [m], G. Gutierrez [at], P. Gutierrez [bp], J. Haley [bq], L. Han [d], K. Harder [ap], A. Harel [bl], J.M. Hauptman [ba], J. Hays [ao], T. Head [ap], T. Hebbeker [s], D. Hedin [av], H. Hegab [bq], A.P. Heinson [ar], U. Heintz [br], C. Hensel [a], I. Heredia-De La Cruz [ac,4], K. Herner [at], G. Hesketh [ap,6], M.D. Hildreth [az], R. Hirosky [bv], T. Hoang [as], J.D. Hobbs [bm], B. Hoeneisen [i], J. Hogan [bu], M. Hohlfeld [v], J.L. Holzbauer [bg], I. Howley [bs], Z. Hubacek [g,o], V. Hynek [g], I. Iashvili [bk], Y. Ilchenko [bt], R. Illingworth [at], A.S. Ito [at], S. Jabeen [at,13], M. Jaffré [m], A. Jayasinghe [bp], M.S. Jeong [ab], R. Jesik [ao], P. Jiang [d], K. Johns [aq], E. Johnson [bf], M. Johnson [at], A. Jonckheere [at], P. Jonsson [ao], J. Joshi [ar], A.W. Jung [at], A. Juste [ak], E. Kajfasz [l], D. Karmanov [ah], I. Katsanos [bh], M. Kaur [x], R. Kehoe [bt], S. Kermiche [l], N. Khalatyan [at], A. Khanov [bq], A. Kharchilava [bk], Y.N. Kharzheev [af], I. Kiselevich [ag], J.M. Kohli [x], A.V. Kozelov [ai], J. Kraus [bg], A. Kumar [bk], A. Kupco [h], T. Kurča [q,r], V.A. Kuzmin [ah], S. Lammers [ax], P. Lebrun [q,r], H.S. Lee [ab], S.W. Lee [ba], W.M. Lee [at], X. Lei [aq], J. Lellouch [n],

E-mail address: kehoe@physics.smu.edu (R. Kehoe).

http://dx.doi.org/10.1016/j.physletb.2015.10.086

0370-2693/© 2015 The Authors. Published by Elsevier B.V. This is an open access article under the CC BY license (http://creativecommons.org/licenses/by/4.0/). Funded by SCOAP[3].

D. Li [n], H. Li [bv], L. Li [ar], Q.Z. Li [at], J.K. Lim [ab], D. Lincoln [at], J. Linnemann [bf], V.V. Lipaev [ai], R. Lipton [at], H. Liu [bt], Y. Liu [d], A. Lobodenko [aj], M. Lokajicek [h], R. Lopes de Sa [at], R. Luna-Garcia [ac,7], A.L. Lyon [at], A.K.A. Maciel [a], R. Madar [t], R. Magaña-Villalba [ac], S. Malik [bh], V.L. Malyshev [af], J. Mansour [u], J. Martínez-Ortega [ac], R. McCarthy [bm], C.L. McGivern [ap], M.M. Meijer [ad,ae], A. Melnitchouk [at], D. Menezes [av], P.G. Mercadante [c], M. Merkin [ah], A. Meyer [s], J. Meyer [u,9], F. Miconi [p], N.K. Mondal [z], M. Mulhearn [bv], E. Nagy [l], M. Narain [br], R. Nayyar [aq], H.A. Neal [be], J.P. Negret [e], P. Neustroev [aj], H.T. Nguyen [bv], T. Nunnemann [w], J. Orduna [bu], N. Osman [l], J. Osta [az], A. Pal [bs], N. Parashar [ay], V. Parihar [br], S.K. Park [ab], R. Partridge [br,5], N. Parua [ax], A. Patwa [bn,10], B. Penning [ao], M. Perfilov [ah], Y. Peters [ap], K. Petridis [ap], G. Petrillo [bl], P. Pétroff [m], M.-A. Pleier [bn], V.M. Podstavkov [at], A.V. Popov [ai], M. Prewitt [bu], D. Price [ap], N. Prokopenko [ai], J. Qian [be], A. Quadt [u], B. Quinn [bg], P.N. Ratoff [an], I. Razumov [ai], I. Ripp-Baudot [p], F. Rizatdinova [bq], M. Rominsky [at], A. Ross [an], C. Royon [o], P. Rubinov [at], R. Ruchti [az], G. Sajot [k], A. Sánchez-Hernández [ac], M.P. Sanders [w], A.S. Santos [a,8], G. Savage [at], M. Savitskyi [am], L. Sawyer [bc], T. Scanlon [ao], R.D. Schamberger [bm], Y. Scheglov [aj], H. Schellman [aw], M. Schott [v], C. Schwanenberger [ap], R. Schwienhorst [bf], J. Sekaric [bb], H. Severini [bp], E. Shabalina [u], V. Shary [o], S. Shaw [ap], A.A. Shchukin [ai], V. Simak [g], P. Skubic [bp], P. Slattery [bl], D. Smirnov [az], G.R. Snow [bh], J. Snow [bo], S. Snyder [bn], S. Söldner-Rembold [ap], L. Sonnenschein [s], K. Soustruznik [f], J. Stark [k], D.A. Stoyanova [ai], M. Strauss [bp], L. Suter [ap], P. Svoisky [bp], M. Titov [o], V.V. Tokmenin [af], Y.-T. Tsai [bl], D. Tsybychev [bm], B. Tuchming [o], C. Tully [bj], L. Uvarov [aj], S. Uvarov [aj], S. Uzunyan [av], R. Van Kooten [ax], W.M. van Leeuwen [ad], N. Varelas [au], E.W. Varnes [aq], I.A. Vasilyev [ai], A.Y. Verkheev [af], L.S. Vertogradov [af], M. Verzocchi [at], M. Vesterinen [ap], D. Vilanova [o], P. Vokac [g], H.D. Wahl [as], M.H.L.S. Wang [at], J. Warchol [az], G. Watts [bw], M. Wayne [az], J. Weichert [v], L. Welty-Rieger [aw], M.R.J. Williams [ax,14], G.W. Wilson [bb], M. Wobisch [bc], D.R. Wood [bd], T.R. Wyatt [ap], Y. Xie [at], R. Yamada [at], S. Yang [d], T. Yasuda [at], Y.A. Yatsunenko [af], W. Ye [bm], Z. Ye [at], H. Yin [at], K. Yip [bn], S.W. Youn [at], J.M. Yu [be], J. Zennamo [bk], T.G. Zhao [ap], B. Zhou [be], J. Zhu [be], M. Zielinski [bl], D. Zieminska [ax], L. Zivkovic [n]

[a] *LAFEX, Centro Brasileiro de Pesquisas Físicas, Rio de Janeiro, Brazil*
[b] *Universidade do Estado do Rio de Janeiro, Rio de Janeiro, Brazil*
[c] *Universidade Federal do ABC, Santo André, Brazil*
[d] *University of Science and Technology of China, Hefei, People's Republic of China*
[e] *Universidad de los Andes, Bogotá, Colombia*
[f] *Charles University, Faculty of Mathematics and Physics, Center for Particle Physics, Prague, Czech Republic*
[g] *Czech Technical University in Prague, Prague, Czech Republic*
[h] *Institute of Physics, Academy of Sciences of the Czech Republic, Prague, Czech Republic*
[i] *Universidad San Francisco de Quito, Quito, Ecuador*
[j] *LPC, Université Blaise Pascal, CNRS/IN2P3, Clermont, France*
[k] *LPSC, Université Joseph Fourier Grenoble 1, CNRS/IN2P3, Institut National Polytechnique de Grenoble, Grenoble, France*
[l] *CPPM, Aix-Marseille Université, CNRS/IN2P3, Marseille, France*
[m] *LAL, Université Paris-Sud, CNRS/IN2P3, Orsay, France*
[n] *LPNHE, Universités Paris VI and VII, CNRS/IN2P3, Paris, France*
[o] *CEA, Irfu, SPP, Saclay, France*
[p] *IPHC, Université de Strasbourg, CNRS/IN2P3, Strasbourg, France*
[q] *IPNL, Université Lyon 1, CNRS/IN2P3, Villeurbanne, France*
[r] *Université de Lyon, Lyon, France*
[s] *III. Physikalisches Institut A, RWTH Aachen University, Aachen, Germany*
[t] *Physikalisches Institut, Universität Freiburg, Freiburg, Germany*
[u] *II. Physikalisches Institut, Georg-August-Universität Göttingen, Göttingen, Germany*
[v] *Institut für Physik, Universität Mainz, Mainz, Germany*
[w] *Ludwig-Maximilians-Universität München, München, Germany*
[x] *Panjab University, Chandigarh, India*
[y] *Delhi University, Delhi, India*
[z] *Tata Institute of Fundamental Research, Mumbai, India*
[aa] *University College Dublin, Dublin, Ireland*
[ab] *Korea Detector Laboratory, Korea University, Seoul, Republic of Korea*
[ac] *CINVESTAV, Mexico City, Mexico*
[ad] *Nikhef, Science Park, Amsterdam, The Netherlands*
[ae] *Radboud University Nijmegen, Nijmegen, The Netherlands*
[af] *Joint Institute for Nuclear Research, Dubna, Russia*
[ag] *Institute for Theoretical and Experimental Physics, Moscow, Russia*
[ah] *Moscow State University, Moscow, Russia*
[ai] *Institute for High Energy Physics, Protvino, Russia*
[aj] *Petersburg Nuclear Physics Institute, St. Petersburg, Russia*
[ak] *Institució Catalana de Recerca i Estudis Avançats (ICREA) and Institut de Física d'Altes Energies (IFAE), Barcelona, Spain*

[al] Uppsala University, Uppsala, Sweden
[am] Taras Shevchenko National University of Kyiv, Kiev, Ukraine
[an] Lancaster University, Lancaster LA1 4YB, United Kingdom
[ao] Imperial College London, London SW7 2AZ, United Kingdom
[ap] The University of Manchester, Manchester M13 9PL, United Kingdom
[aq] University of Arizona, Tucson, AZ 85721, USA
[ar] University of California Riverside, Riverside, CA 92521, USA
[as] Florida State University, Tallahassee, FL 32306, USA
[at] Fermi National Accelerator Laboratory, Batavia, IL 60510, USA
[au] University of Illinois at Chicago, Chicago, IL 60607, USA
[av] Northern Illinois University, DeKalb, IL 60115, USA
[aw] Northwestern University, Evanston, IL 60208, USA
[ax] Indiana University, Bloomington, IN 47405, USA
[ay] Purdue University Calumet, Hammond, IN 46323, USA
[az] University of Notre Dame, Notre Dame, IN 46556, USA
[ba] Iowa State University, Ames, IA 50011, USA
[bb] University of Kansas, Lawrence, KS 66045, USA
[bc] Louisiana Tech University, Ruston, LA 71272, USA
[bd] Northeastern University, Boston, MA 02115, USA
[be] University of Michigan, Ann Arbor, MI 48109, USA
[bf] Michigan State University, East Lansing, MI 48824, USA
[bg] University of Mississippi, University, MS 38677, USA
[bh] University of Nebraska, Lincoln, NE 68588, USA
[bi] Rutgers University, Piscataway, NJ 08855, USA
[bj] Princeton University, Princeton, NJ 08544, USA
[bk] State University of New York, Buffalo, NY 14260, USA
[bl] University of Rochester, Rochester, NY 14627, USA
[bm] State University of New York, Stony Brook, NY 11794, USA
[bn] Brookhaven National Laboratory, Upton, NY 11973, USA
[bo] Langston University, Langston, OK 73050, USA
[bp] University of Oklahoma, Norman, OK 73019, USA
[bq] Oklahoma State University, Stillwater, OK 74078, USA
[br] Brown University, Providence, RI 02912, USA
[bs] University of Texas, Arlington, TX 76019, USA
[bt] Southern Methodist University, Dallas, TX 75275, USA
[bu] Rice University, Houston, TX 77005, USA
[bv] University of Virginia, Charlottesville, VA 22904, USA
[bw] University of Washington, Seattle, WA 98195, USA

ARTICLE INFO

Article history:
Received 13 August 2015
Received in revised form 19 October 2015
Accepted 31 October 2015
Available online 11 November 2015
Editor: H. Weerts

ABSTRACT

We measure the top quark mass in dilepton final states of $t\bar{t}$ events in $p\bar{p}$ collisions at $\sqrt{s} = 1.96$ TeV, using data corresponding to an integrated luminosity of 9.7 fb^{-1} at the Fermilab Tevatron Collider. The analysis features a comprehensive optimization of the neutrino weighting method to minimize the statistical uncertainties. We also improve the calibration of jet energies using the calibration determined in $t\bar{t} \to$ lepton + jets events, which reduces the otherwise limiting systematic uncertainty from the jet energy scale. The measured top quark mass is $m_t = 173.32 \pm 1.36(\text{stat}) \pm 0.85(\text{syst})$ GeV.

© 2015 The Authors. Published by Elsevier B.V. This is an open access article under the CC BY license (http://creativecommons.org/licenses/by/4.0/). Funded by SCOAP[3].

1. Introduction

The discovery of the top quark in 1995 [1,2] completed the three quark families of the standard model (SM). Since then, the top quark has been one of the focal points of the Fermilab Tevatron and of the CERN LHC programs. The top quark stands out because of its large mass, m_t, which is a fundamental parameter in the SM. Its Yukawa coupling to the Higgs boson, $Y_t = \sqrt{2}m_t/v$, where v is the vacuum expectation value of the Higgs field, is close to unity, implying that the top quark may play a special role in electroweak symmetry breaking. In addition, m_t is linked to the W and Higgs boson masses, M_W and M_H, through radiative corrections [3]. Following the Higgs boson discovery [4,5], a precise measurement of m_t provides a test of the electroweak sector of the SM and information on whether our universe resides in a stable or metastable region of that theory [6–8]. The short lifetime of the top quark prevents its confinement in the strong color field, since top quarks decay before hadronizing. This allows a particularly precise study of pure quantum chromodynamic (QCD) effects. A comparison of the measured m_t and the m_t extracted from cross section mea-

[1] Visitor from Augustana College, Sioux Falls, SD, USA.
[2] Visitor from The University of Liverpool, Liverpool, UK.
[3] Visitor from DESY, Hamburg, Germany.
[4] Visitor from CONACyT, Mexico City, Mexico.
[5] Visitor from SLAC, Menlo Park, CA, USA.
[6] Visitor from University College London, London, UK.
[7] Visitor from Centro de Investigacion en Computacion – IPN, Mexico City, Mexico.
[8] Visitor from Universidade Estadual Paulista, São Paulo, Brazil.
[9] Visitor from Karlsruher Institut für Technologie (KIT) – Steinbuch Centre for Computing (SCC), D-76128 Karlsruhe, Germany.
[10] Visitor from Office of Science, U.S. Department of Energy, Washington, D.C. 20585, USA.
[11] Visitor from American Association for the Advancement of Science, Washington, D.C. 20005, USA.
[12] Visitor from Kiev Institute for Nuclear Research, Kiev, Ukraine.
[13] Visitor from University of Maryland, College Park, Maryland 20742, USA.
[14] Visitor from European Organization for Nuclear Research (CERN), Geneva, Switzerland.

surements [9–12] may provide a probe of higher order and soft QCD corrections to the observed mass [13].

Assuming the SM branching ratio of $t \to Wb \approx 100\%$, $t\bar{t}$ decays yield distinct final state categories according to the number of charged leptons with high transverse momentum (p_T) from W boson decays. Dilepton (2ℓ, $\ell = e$ or μ) events, such as ee, $e\mu$, and $\mu\mu$, with neutrinos from two $W \to \ell\nu$ decays, are relatively rare but have low background. We present a measurement of m_t using $p\bar{p}$ collider data collected with the D0 detector at the Fermilab Tevatron collider, corresponding to an integrated luminosity of 9.7 fb^{-1}, in events with two high-p_T electrons or muons of opposite electric charge. Two high-p_T jets must also be observed, one of which must be identified as being consistent with originating from a b quark. This analysis is based on our previous dilepton measurement [14], but with increased integrated luminosity and multiple optimizations to improve the precision of m_t. We reduce the dominant statistical contribution to the uncertainty on m_t through an optimization of the methods for kinematic reconstruction and statistical analysis. Lacking a dijet signature from $W \to q\bar{q}'$, which is present in $t\bar{t} \to$ lepton + jets (ℓ + jets) events and was used to improve the precision of jet energy calibration with a W mass constraint [15], previous dilepton analyses at the Tevatron have reached a sensitivity limit imposed by standard jet calibration methods [16,17]. Progress in calibrating jet energies in the dilepton channel [14] provides improved cross-checks across different channels and a more significant contribution from the dilepton channel to the world average m_t [18]. For comparison, the most recent measurements of m_t in the dilepton channel from CDF, ATLAS, and CMS are, respectively, $m_t = 171.5 \pm 1.9(\text{stat}) \pm 2.5(\text{syst})$ GeV [19], $m_t = 173.79 \pm 0.54(\text{stat}) \pm 1.30(\text{syst})$ GeV [20], and $m_t = 172.50 \pm 0.43(\text{stat}) \pm 1.46(\text{syst})$ GeV [21]. In this analysis, we substantially reduce the otherwise dominant uncertainty in the jet energy scale by applying the methods of Ref. [14].

2. Detector and data sample

2.1. Detector

The D0 detector [22,23] has a central-tracking system, consisting of a silicon microstrip tracker and a central fiber tracker, both located within a 1.9 T superconducting solenoidal magnet, with designs optimized for identification of the $p\bar{p}$ collision vertex and track reconstruction at pseudorapidities [24] of $|\eta| < 3$ and $|\eta| < 2.5$, respectively. The liquid-argon/uranium calorimeter has a central section covering $|\eta| \leq 1.1$, and two end sections that extend coverage to $|\eta| \approx 4.2$, with all three housed in separate cryostats. An outer muon system, covering $|\eta| < 2$, consists of a layer of tracking detectors and scintillation trigger counters in front of 1.8 T iron toroids, followed by two similar layers after the toroids.

2.2. Object reconstruction

We require electrons to satisfy an identification criterion based on boosted decision trees [25] using calorimeter and tracking information. Muons must satisfy requirements that match hits in the muon system to a track in the central tracking detector that is required to have a small distance of closest approach to the beam axis [26]. We require hits in the muon layers inside and outside the toroid. Muons and charged hadron momenta are measured in the central tracking detector, while electron, photon (γ), jet, and charged hadron energies are measured in the calorimeters. Muons must be isolated from jets and from nearby tracks. Electrons and muons must have their extrapolated track trajectories isolated from calorimeter energy depositions greater than an energy threshold. Electrons and muons must have $p_T > 15$ GeV, and $|\eta| < 2.5$ and < 2.0, respectively. We reconstruct jets using an iterative, midpoint-seeded cone algorithm with a cone parameter of $\mathcal{R}_{\text{cone}} = 0.5$ [27]. Jets with embedded muons from the decay of b-hadrons require an additional correction to jet energy to account for the associated neutrino. A multivariate discriminant [28] is used to identify jets that contain a b-hadron (i.e., b jets) from a vertex displaced from the interaction point. We define the missing transverse momentum ($\not\!\!E_T$) attributed to the escaping neutrinos as the negative of the vector sum of all transverse components of calorimeter cell energies, corrected for the measured muon momenta and the response of the calorimeter to electrons. We also correct $\not\!\!E_T$ for detector response in the jet energy calibration, as described below. Details of object reconstruction are provided in Ref. [29].

2.3. Standard jet energy calibration

We calibrate the energy of jets to be the energy of the particle jets reconstructed using the midpoint algorithm [27]. We correct for the effects of the calorimeter response to particle constituents of jets, energy leaking into the cone from particles directed outside it, as well as energy deposits outside the cone from particles inside it [30]. Charged hadrons have an energy-dependent response that is lower than that of electrons and photons. We therefore apply corrections obtained from γ + jet events to account for the energy dependence of the jet response in the central $|\eta|$ region. We also apply a relative η-dependent correction obtained from γ + jet and dijet events. We employ the same methods to calibrate jet energies independently in the Monte Carlo (MC) simulation and in data. The MC is used to help study potential biases in the data. We incorporate a correction for jets in the MC simulation that accounts for the difference in single-particle response between data and MC. This procedure ensures that the flavor dependence of the jet response in data is replicated in MC. In the MC we account for multiple $p\bar{p}$ interactions by correcting the jet energy to the particle level of only those particles that are directed within the jet cone at particle level. The typical systematic uncertainty in the energy calibration of each jet in the dilepton sample is 2%. This precision is limited by systematic uncertainties of the γ + jet method in the p_T range of jets in $t\bar{t}$ events. Details about this "standard jet energy scale" calibration can be found in Ref. [30]. We require that jets have $p_T > 20$ GeV and $|\eta| < 2.5$ after calibration, but before applying additional corrections from the $W \to q\bar{q}'$ constraint in the ℓ + jets channel discussed below.

3. Absolute jet calibration from a $W \to q\bar{q}'$ constraint

As in Ref. [14], we apply a multiplicative correction factor to the energy of jets in data based on an analysis of $t\bar{t} \to \ell$ + jets events using the $W \to q\bar{q}'$ decays as a constraint. Application of this factor, $1.0250 \pm 0.0046\,(\text{stat})$ [15], improves the agreement between MC and data and allows us to use its uncertainty to reduce the uncertainty on the absolute energy scale by a factor of ≈ 4 relative to the standard jet energy scale, while retaining its η and p_T dependence. To apply this scale, which comes from light-quark jets, to the dilepton sample, which has b jets, it is important to ensure that the variation in the ratio of data over MC jet response between different flavors be placed on an equal footing. The standard jet energy scale [30] achieves this on a jet-by-jet basis by using single particles in MC jets to correct the simulation so that it has the same kinematic and flavor-dependent jet response as that in data. This ensures that the energies of b jets in dilepton simulated samples agree with those of b jets in the dilepton data sample at the same level as light-quark jets. Aside from fragmentation differences between data and MC which are discussed below, this

approach justifies the use of the ℓ + jets constraint in the dilepton channel.

4. Event selection

The $t\bar{t}$ candidate events in the ee and $\mu\mu$ channels are required to pass single-lepton triggers. The full suite of triggers is used for selecting $e\mu$ events. The dilepton event selection before optimization is described in Ref. [29]. We optimize the selection based on MC events to provide the smallest expected statistical uncertainty in m_t. We require two isolated leptons with opposite electric charge. We require at least two jets, where at least one of the two jets with highest p_T must be identified as a b jet. For the $e\mu$ channel, our selections have an efficiency for tagging b jets of 72%, and a light-quark mistag rate of 12% in the central region in η. The same-flavor channels employ slightly tighter b tagging requirements and thus have a few percent lower efficiency, and 30% lower mistag rate. We require events in the $\mu\mu$ channel to have $\not\!\!E_T > 40$ GeV. This $\not\!\!E_T$ selection is also applied to ee events when the dielectron invariant mass is between 70 and 100 GeV, to reduce the $Z \to ee$ background contribution. We define a $\not\!\!E_T$ significance variable, $\mathcal{S}$, which measures the likelihood for the observed $\not\!\!E_T$ to be a fluctuation from $\not\!\!E_T = 0$ GeV. We require $\mathcal{S} > 3.5$ (4) for the ee ($\mu\mu$) channel. We require $e\mu$ events to have $H_T > 100$ GeV, where H_T is the scalar sum of the p_T of the two highest-p_T jets and of the lepton with highest p_T. The H_T, b tagging, and $\not\!\!E_T$-based requirements are optimized to minimize the expected statistical uncertainty on m_t in each channel. The expected signal-to-background (S/B) ratio is ≈ 7 for these channels. These requirements yield a 3% improvement in statistical precision in m_t relative to the selections in Ref. [14]. After implementing all these selections, we obtain 340, 115, and 110 events in the $e\mu$, ee and $\mu\mu$ channels, respectively.

5. Modeling signal and background

The $t\bar{t}$ events are simulated at 15 mass points over the range $130 \leq m_t^{\rm MC} \leq 200$ GeV using the tree level generator ALPGEN 2.11 [31] with up to 2 additional light partons and PYTHIA 6.409 [32] with modified underlying event Tune A for parton showering and hadronization. Here, $m_t^{\rm MC}$ refers to the input mass in ALPGEN. An additional, larger sample is generated at $m_t^{\rm MC} = 172.5$ GeV to study systematic uncertainties. We normalize the $t\bar{t}$ production cross section to $\sigma_{t\bar{t}} = 7.24 \pm 0.23$ pb [33], which is calculated at next-to-next-to-leading order with a next-to-next-to-leading logarithm soft gluon resummation. The main backgrounds arise from three sources: $Z/\gamma^* \to \ell^+\ell^-$, diboson ($WW$, WZ, and ZZ) processes, and instrumental effects. We model the Z/γ^* background using ALPGEN with up to 2 light partons and PYTHIA for showering and hadronization. We employ PYTHIA for the diboson background. The instrumental background arises from W + jets, multijet, or ℓ + jets $t\bar{t}$ events where one or two jets are either mis-identified as electrons, or they contain a hadron decaying to a non-isolated lepton that passes our selection. This background is estimated from data as in Ref. [29]. We apply a full detector simulation based on GEANT 3.14 [34] for all simulated events. The objects reconstructed in simulation are smeared to ensure that their resolutions reflect those in data. Scale factors in object efficiencies are applied to improve agreement between data and MC.

6. Kinematic reconstruction

6.1. Neutrino weighting

The presence of two neutrinos in the $t\bar{t}$ decay makes it impossible to fully constrain the kinematics and thus extract a unique m_t measurement from each event. Given the measured momenta of leptons, jets and $\not\!\!E_T$, the available constraints from M_W, and the condition $m_t = m_{\bar{t}}$, we are missing one constraint to provide full $t\bar{t}$ reconstruction in dilepton events. We integrate over the phase space of neutrino rapidities for chosen values of hypothesized m_t (m_t^h) [35], and compare $\not\!\!E_T^{\rm calc}$, the vector sum of neutrino momentum solutions at each chosen point of phase space, to the observed $\not\!\!E_T^{\rm obs}$ to determine a "weight" ω characterizing the level of agreement:

$$\omega = \frac{1}{N}\sum_{i=1}^{N}\prod_{j=x,y}\exp\left(-\frac{(\not\!\!E_{j,i}^{\rm calc} - \not\!\!E_j^{\rm obs})^2}{2\sigma_{\not\!\!E_T}^2}\right), \quad (1)$$

where i runs over all neutrino solutions for any two possible jet-lepton assignments in the $t\bar{t}$ final state (up to $N = 8$), j stands for the two orthogonal coordinates in the transverse plane (x and y), and $\sigma_{\not\!\!E_T}$ is a parameter representing the RMS of the difference between the transverse components of the measured $\not\!\!E_T$ and the sum of the solved neutrino transverse momenta. The parameter $\sigma_{\not\!\!E_T}$ is taken to be the same in both x and y directions. We perform this calculation over a range of m_t^h, integrating ω over the neutrino phase space, to yield a distribution of $\omega(m_t)$ versus m_t^h. Prior studies [36] have shown that the first two moments $(\mu_\omega, \sigma_\omega)$ of this distribution extract most of the information about m_t. The analysis of Ref. [14] used the range of m_t^h values between 80 and 330 GeV in 1 GeV steps and a $\sigma_{\not\!\!E_T}$ of 7 GeV in the weight calculation. The new optimized determination of these parameters is briefly summarized below.

6.2. Optimization of weight calculation parameters

After applying the methods described above to improve the jet energy calibration, the statistical contribution is the dominant source of measurement uncertainty on m_t in the dilepton channel. We therefore examine the parameters used for the kinematic reconstruction of $t\bar{t}$ events and for the maximum likelihood fit to reduce the expected statistical uncertainty. At each step, we verify through MC simulations that the optimization does not increase the systematic uncertainty.

All neutrino solutions and jet assignments yield mass estimators such as μ_ω that are correlated with m_t. However, the correlation is substantially greater, and μ_ω values are less biased, when the correct jet assignments and solutions of neutrino momenta are chosen. Since now m_t has been measured with high precision [18], we can optimize the range of m_t^h based on known values of m_t. Considering a wide range in m_t^h causes incorrect configurations to overwhelm the correct configuration, thereby worsening the mass resolution. Likewise, scanning over too narrow a range biases the background and worsens the mass sensitivity by causing $t\bar{t}$ and background distributions to be similar. Examination of a two-dimensional grid of upper and lower limits of the mass range yields the optimal range of $m_t^h = 115$ to 220 GeV in 1 GeV steps. The value of $\sigma_{\not\!\!E_T}$ also has a noticeable impact on the expected precision of the analysis. This was not the case in Ref. [14], mainly because the final top quark mass measurement was less precise. In Ref. [14], the value of 7 GeV for $\sigma_{\not\!\!E_T}$ was obtained as the unclustered $\not\!\!E_T$ resolution in an earlier dataset [36], where the unclustered $\not\!\!E_T$ is the magnitude of the vector sum of all energy depositions in the calorimeter that are not included in lepton or jet reconstruction. However, accounting only for the unclustered energy resolution as the origin of the difference between the calculated and measured $\not\!\!E_T$ ignores the effect of assumptions that go into the kinematic reconstruction. For instance, the finite binning of the neutrino rapidities discretizes the solved neutrino momenta and therefore the solved $\not\!\!E_T$. Also, the solved $\not\!\!E_T$ does not include

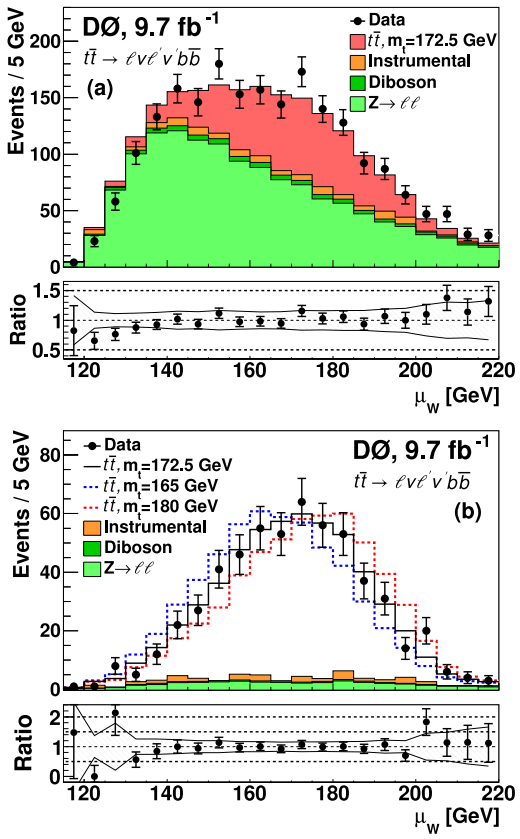

Fig. 1. The distribution in the mass estimator, μ_w, for the combination of the ee, $e\mu$, and $\mu\mu$ channels for (a) the preselected sample and (b) the final event sample. The MC events are normalized separately to the number of observed events in data in each channel. The ratios show the total number of observed events divided by the number of expected events in a given bin of μ_w for $m_t^{\mathrm{MC}} = 172.5$ GeV. The band of systematic uncertainty is shown as the shaded area in the ratio plots, which includes contributions from the dominant sources: jet energy scale, lepton identification, lepton momentum scale, luminosity, b quark modeling, initial and final state radiation, color reconnection, as well as hadronization and higher-order QCD effects for $t\bar{t}$ events.

additional jets, reconstructed or not, since only the two leading jets are considered in the kinematic reconstruction. Due to these additional contributions, a scan in a wide range from 7 to 100 GeV is performed and we find the optimal value for $\sigma_{\not\!\!E_T}$ to be 25 GeV, which is larger than the 7 GeV of Ref. [14]. Combined, these optimizations improve the expected combined statistical uncertainty on m_t by 11% compared to the parameters in Ref. [14].

6.3. Efficiency of kinematic reconstruction and event yields

Events used in the analysis must have at least one pair of neutrino solutions for at least one m_t^h value. The efficiency for this kinematic reconstruction is over 99% for $t\bar{t}$ events, and 91% to 98% for the background. In the final sample, a total of 336, 113, and 109 events in the $e\mu$, ee, and $\mu\mu$ channels, respectively, pass the kinematic reconstruction. The expected sum of $t\bar{t}$ and background yields and their corresponding asymmetric total uncertainties (stat $\oplus$ syst) are $298.1^{+22.1}_{-27.2}$, $106.5^{+10.4}_{-11.6}$, and $103.5^{+7.4}_{-9.1}$ events for the $e\mu$, ee, and $\mu\mu$ channels, respectively. The distributions of the mass estimator μ_ω in a preselected sample, omitting requirements on b tagging, $\not\!\!E_T$, $\not\!\!E_T$ significance, and H_T, are shown in Fig. 1(a). The $t\bar{t}$ component is evident in the preselected data. The mass dependence of the μ_ω distribution is given in Fig. 1(b) for three m_t^{MC} mass points with all selections applied.

7. Extracting the top quark mass

7.1. Maximum likelihood

We perform a binned maximum likelihood fit to the extracted moment distributions $[\mu_\omega, \sigma_\omega]$ in data. Expected probability densities are calculated using the MC samples for each of the 16 m_t points, yielding a two-dimensional probability density $h_{\mathrm{S}}(\mu_\omega, \sigma_\omega | m_t^{\mathrm{MC}})$ distribution parametrized by m_t. Background samples are used to construct a background template for each channel, $h_{\mathrm{B}}(\mu_\omega, \sigma_\omega)$, with each background contributing according to its expected yield. Bins in signal templates with no events are given a weighted value corresponding to a single signal MC event to ensure that the log of likelihood is not infinite. The likelihood is given by:

$$\mathcal{L}(\mu_{\omega\{1..N\}}, \sigma_{\omega\{1..N\}}, N \mid n_{\mathrm{S}}, n_{\mathrm{B}}, m_t) = \prod_{i=1}^{N} \frac{n_{\mathrm{S}} \cdot h_{\mathrm{S}}(\mu_{\omega i}, \sigma_{\omega i} \mid m_t) + n_{\mathrm{B}} \cdot h_{\mathrm{B}}(\mu_{\omega i}, \sigma_{\omega i})}{n_{\mathrm{S}} + n_{\mathrm{B}}}, \tag{2}$$

where N is the number of observed events in data, n_{S} is the expected number of $t\bar{t}$ events (for $m_t = 172.5$ GeV), and n_{B} is the expected total number of background events. We fit $(-\ln \mathcal{L})$ versus m_t^{MC} to a parabola in a window of m_t^{MC} that is iteratively varied until a stable minimum is found. We take the minimum of the final parabola to be the fitted top quark mass, m_t^{fit}. The uncertainty on the fitted mass is obtained by considering the m_t^{MC} range over which the fit function increases by 0.5 units in $(-\ln \mathcal{L})$ above this minimum. Using pseudo-experiments, we optimize the template binning of each channel separately in a two-dimensional grid that lets μ_ω and σ_ω bin sizes vary independently. Finer binning in μ_ω and σ_ω, especially for the $e\mu$ channel, improves the expected statistical precision in m_t^{fit} by 5%. The fitted mass window is optimized to ± 15 GeV for all channels. Taking all the optimizations together, including event selection, weight calculation, and maximum likelihood fitting, the statistical sensitivity of this analysis is improved relative to Ref. [14] by 20% beyond the 35% gain expected from increased integrated luminosity.

7.2. Ensemble testing and data results

We obtain a linear relationship between m_t^{fit} and m_t^{MC} by performing randomized pseudo-experiments using all signal mass points. The numbers of signal and background events in the pseudo-experiments are allowed to fluctuate within their Poisson uncertainties around their expected values. We require that the total number of events matches that observed in data. To minimize the effect of statistical fluctuations on our systematic uncertainties, we optimize the number of pseudo-experiments by dividing the MC sample into five subsamples, and measure systematic uncertainties with each subsample. We calculate the RMS of the five uncertainties, average over all systematic effects, and divide by $\sqrt{5}$ to estimate the statistical component of systematic uncertainties. The average RMS decreases until we oversample, or reuse, the $t\bar{t}$ MC events by roughly a factor of three. This corresponds to 3000 pseudo-experiments. We perform a linear fit of m_t^{fit} versus m_t^{MC} to obtain a calibration slope and offset for m_t^{fit} using 3000 pseudo-experiments:

$$m_t^{\mathrm{fit}} = \mathrm{Slope} \cdot (m_t^{\mathrm{MC}} - 170) + \mathrm{Offset} + 170. \tag{3}$$

We account for oversampling by increasing the statistical uncertainties at each mass point by the appropriate oversampling factor. Likewise, we compute the pull, or the ratio of $m_t^{\mathrm{fit}} - m_t^{\mathrm{MC}}$ over the average estimated uncertainty at each mass point. The slopes

Table 1
Slopes, offsets, and pull widths of the m_t calibration and the expected statistical uncertainties in the mass (σ_{m_t}) for the ee, $e\mu$, and $\mu\mu$ channels, and their combination.

	Slope	Offset [GeV]	Pull width	σ_{m_t} [GeV]
ee	0.984 ± 0.004	0.671 ± 0.043	0.994	2.98
$e\mu$	0.986 ± 0.006	0.548 ± 0.065	0.998	1.72
$\mu\mu$	0.989 ± 0.010	0.717 ± 0.103	1.004	3.31
2ℓ	0.988 ± 0.006	0.617 ± 0.063	0.995	1.35

Table 2
Systematic uncertainties on m_t for the combined dilepton measurement using 9.7 fb^{-1} of integrated luminosity. For symmetrized uncertainties, the "$\pm$" symbol indicates that the corresponding systematic parameters in MC are positively correlated with m_t in data, and the "$\mp$" symbol indicates an anticorrelation. The uncertainties shown as $+$ or $-$ only are computed by comparing a standard choice with an alternate, but are symmetrized in calculating the total uncertainty.

Source	σ_{m_t} [GeV]
Jet energy calibration	
Absolute scale	∓ 0.47
Flavor dependence	∓ 0.27
Residual scale	$^{+0.36}_{-0.35}$
b quark fragmentation	$+0.10$
Object reconstruction	
Trigger	-0.06
Electron p_T resolution	± 0.01
Muon p_T resolution	∓ 0.03
Electron energy scale	± 0.01
Muon p_T scale	± 0.01
Jet resolution	∓ 0.12
Jet identification	$+0.03$
b tagging	∓ 0.19
Signal modeling	
Higher-order effects	-0.33
ISR/FSR	± 0.15
$p_T(t\bar{t})$	-0.07
Hadronization	-0.11
Color reconnection	-0.22
Multiple $p\bar{p}$ interactions	-0.06
PDF uncertainty	± 0.08
Background modeling	
Signal fraction	± 0.01
Heavy-flavor scale factor	± 0.04
Method	
Template statistics	± 0.18
Calibration	± 0.07
Total systematic uncertainty	± 0.85

of m_t^{fit} versus m_t^{MC} are close to 1, and pull widths are consistent with unity, as shown in Table 1. We calculate the final m_t by correcting m_t^{fit} from a given measurement by the slope and offset. We correct the statistical uncertainty using the slope and the pull width. The expected corrected statistical uncertainties for each channel are given in Table 1. In data, we obtain corrected, fitted m_t values of $m_t = 171.86 \pm 1.71(\text{stat})$, $173.99 \pm 3.04(\text{stat})$, and $178.58 \pm 3.56(\text{stat})$ GeV for the $e\mu$, ee, and $\mu\mu$ channels respectively, and $m_t = 173.32 \pm 1.36(\text{stat})$ GeV for the combined channels.

8. Systematic uncertainties

Systematic uncertainties summarized in Table 2 arise from jet energy calibration, object reconstruction, modeling of $t\bar{t}$ and background events, and the mass-extraction method. The energies of jets are shifted up and down by the uncertainty on the absolute energy scale, which is taken from $\ell +$ jets events, thereby providing shifts in m_t. This scale is appropriate for light-quark jets, which, after correcting for jet flavors to improve the agreement between data and MC, have different kinematic distributions than b jets from $t\bar{t}$ decays. We calculate a residual uncertainty due to the kinematic differences between the $\ell +$ jets calibration sample and dilepton sample of b jets. We use separate up and down estimates to extract the energy- and η-dependent shifts in m_t based on uncertainties in the standard jet energy scale relative to their average value in the $\ell +$ jets calibration sample. We cross-check this with an alternative method that applies shifted light-quark jet energy scales to b jets in the $\ell +$ jets channel [15]. These methods agree, and thereby validate the use of the $\ell +$ jets scale as a jet calibration. We also cross-check using a jet-energy-dependent linear parameterization of the residual jet energy scale as in Ref. [15], obtaining results that do not exceed our estimate of uncertainties from the jet energy scale. To estimate the uncertainty corresponding to possible differences in the flavor dependence of the MC scale relative to data, we change the single-particle responses up and down by their uncertainties and obtain the shift in m_t. To estimate the possible dependence on the b quark fragmentation in the MC, we replace the PYTHIA b quark fragmentation function with the Bowler scheme [37], and compare m_t with the Bowler free parameters tuned to LEP (ALEPH, OPAL, and DELPHI) or SLD data [38].

The systematic uncertainty due to the trigger efficiency is estimated by applying the ratio of single lepton trigger efficiency parameterization in data divided by the MC parameterization to the ee and $\mu\mu$ channels. The uncertainties in the modeling of the energy and momentum resolutions of electrons, muons, and jets are applied independently of each other, and the shifts in m_t are extracted as uncertainties on m_t. Lepton energy or momentum scales and their uncertainties are extracted from $Z \to 2\ell$ events in data. An additional uncertainty is estimated for jet identification by shifting the jet identification efficiency within its uncertainty in MC samples to estimate their effect on m_t. The uncertainty from modeling b tagging is evaluated by changing within their uncertainties the corrections that account for the agreement between data and MC in b tagging efficiency.

Higher-order virtual corrections to m_t are absent in the ALPGEN used to generate our standard $t\bar{t}$ samples. We therefore compare an ensemble of pseudo-experiments using MC@NLO 3.4 [39] $t\bar{t}$ events with one using ALPGEN events, where both employ HERWIG 6.510 [40] for modeling of hadronization. To evaluate the uncertainty associated with the modeling of initial and final-state radiation (ISR/FSR), we compare ALPGEN+PYTHIA with the renormalization and factorization scale changed up and down by a factor of 1.5 [15]. The $\ell +$ jets analysis exhibits a discrepancy in the shape of the p_T distribution of the $t\bar{t}$ system, which, although the dilepton statistics are limited, may be present in the dilepton sample. We evaluate the uncertainty in the modeling of the $t\bar{t}$ p_T distribution by reweighting MC events to make them match the data. The observed shift in m_t is taken as the uncertainty. Since the hadronization in our standard $t\bar{t}$ sample is modeled with PYTHIA, we estimate a hadronization uncertainty on m_t by performing pseudo-experiments using an ALPGEN+HERWIG sample. We evaluate the effect of color reconnection by comparing m_t measurements in ALPGEN+PYTHIA samples with two PYTHIA tunes: the Perugia2011 tune that incorporates an explicit color-reconnection scheme, and the Perugia2011 NOCR tune that does not [41]. Data and MC may have different distributions in instantaneous luminosity after event selection. This uncertainty due to multiple $p\bar{p}$ interactions is estimated by reweighting the distribution of instantaneous luminosity to make MC agree with the data for respective data-taking epochs, and then take the shift in m_t with respect to the default value. The uncertainty due to the proton structure is obtained from the 20 sets of CTEQ6L1 parton distribution functions (PDF) reweighted

to CTEQ6M, where the deviations in m_t for the 20 eigenvectors sets are added in quadrature [42].

We estimate the effect of the uncertainty on the fraction of signal or background by changing the expected $t\bar{t}$ event yields (n_S) up and down and the expected background yields (n_B) down and up within their total uncertainties. The heavy-flavor scale factor, which is applied to the $Z \to 2\ell$ cross section to correct the heavy-flavor content, is also changed up and down within its uncertainty to estimate its systematic effect on m_t.

Our templates are constructed from MC samples for $t\bar{t}$, $Z \to 2\ell$, and diboson backgrounds, as well as data samples for instrumental background, yielding statistical uncertainties on their bin contents. We use Poisson distributions to modify bin contents within their statistical uncertainties to obtain 1000 new templates. We measure m_t in data using these templates, and the RMS of the measured top quark mass is taken as its uncertainty. Our method of m_t extraction relies on the correction of the fitted m_t to the input MC mass. The uncertainties from this calibration are applied to provide the uncertainty in m_t. The uncertainty is reduced substantially from Ref. [14] due primarily to the reduction in the uncertainty in jet energy calibration and the optimizations for improvements in statistical uncertainty. Larger MC samples also contribute by lowering statistical fluctuations on systematic uncertainties, or reducing statistically limited systematic uncertainties.

9. Conclusions

We have measured the top quark mass in the combined dilepton channels ($e\mu$, ee, $\mu\mu$):

$$m_t = 173.32 \pm 1.36(\text{stat}) \pm 0.85(\text{syst}) \text{ GeV}$$
$$= 173.32 \pm 1.60 \text{ GeV}.$$

This measurement is consistent with the current world average value of m_t [18]. Our measurement is the most precise dilepton result from the Tevatron, and is competitive with the most recent LHC dilepton measurements. The systematic uncertainty of 0.49% is the smallest of all dilepton measurements.

We thank the staffs at Fermilab and collaborating institutions, and acknowledge support from the Department of Energy and National Science Foundation (United States of America); French Alternative Energies and Atomic Energy Commission and National Center for Scientific Research/National Institute of Nuclear and Particle Physics (France); Ministry of Education and Science of the Russian Federation, National Research Center "Kurchatov Institute" of the Russian Federation, and Russian Foundation for Basic Research (Russia); National Council for the Development of Science and Technology and Carlos Chagas Filho Foundation for Research Support in the State of Rio de Janeiro (Brazil); Department of Atomic Energy and Department of Science and Technology (India); Administrative Department of Science, Technology and Innovation (Colombia); National Council of Science and Technology (Mexico); National Research Foundation of Korea (Korea); Foundation for Fundamental Research on Matter (The Netherlands); Science and Technology Facilities Council and The Royal Society (United Kingdom); Ministry of Education, Youth and Sports (Czech Republic); Bundesministerium für Bildung und Forschung (Federal Ministry of Education and Research) and Deutsche Forschungsgemeinschaft (German Research Foundation) (Germany); Science Foundation Ireland (Ireland); Swedish Research Council (Sweden); China Academy of Sciences and National Natural Science Foundation of China (China); and Ministry of Education and Science of Ukraine (Ukraine).

References

[1] S. Abachi, et al., D0 Collaboration, Observation of the top quark, Phys. Rev. Lett. 74 (1995) 2632.
[2] F. Abe, et al., CDF Collaboration, Observation of top quark production in $p\bar{p}$ collisions with the Collider Detector at Fermilab, Phys. Rev. Lett. 74 (1995) 2626.
[3] The Gfitter Group, Results for the global electroweak standard model fit, http://project-gfitter.web.cern.ch/project-gfitter/Standard_Model/.
[4] G. Aad, et al., ATLAS Collaboration, Observation of a new particle in the search for the standard model Higgs boson, Phys. Lett. B 716 (2012) 1.
[5] S. Chatrchyan, et al., CMS Collaboration, Observation of a new boson at a mass of 125 GeV with the CMS experiment at the LHC, Phys. Lett. B 716 (2012) 30.
[6] G. Degrassi, et al., Higgs mass and vacuum stability in the standard model at NNLO, J. High Energy Phys. 08 (2012) 098.
[7] A. De Simone, et al., Running inflation in the standard model, Phys. Lett. B 678 (2009) 1.
[8] F. Bezrukov, et al., The standard model Higgs boson as the inflaton, Phys. Lett. B 659 (2008) 703.
[9] V.M. Abazov, et al., D0 Collaboration, Determination of the pole and $\overline{MS}$ masses of the top quark from the $t\bar{t}$ cross section, Phys. Lett. B 703 (2011) 422.
[10] T. Aaltonen, et al., CDF Collaboration, Cross-section-constrained top-quark mass measurement from dilepton events at the tevatron, Phys. Rev. Lett. 100 (2008) 062005.
[11] S. Chatrchyan, et al., CMS Collaboration, Determination of the top-quark pole mass and strong coupling constant from the $t\bar{t}$ production cross section in pp collisions at $\sqrt{s} = 7$ TeV, Phys. Lett. B 728 (2014) 496.
[12] G. Aad, et al., ATLAS Collaboration, Measurement of the $t\bar{t}$ production cross-section using $e\mu$ events with b-tagged jets in pp collisions at $\sqrt{s} = 7$ and 8 TeV with the ATLAS detector, Eur. Phys. J. C 74 (2014) 3109.
[13] F. Jegerlehner, M. Kalmykov, B. Kniehl, On the difference between the pole and the masses of the top quark at the electroweak scale, Phys. Lett. B 722 (2013) 123.
[14] V.M. Abazov, et al., D0 Collaboration, Measurement of the top quark mass in $p\bar{p}$ collisions using events with two leptons, Phys. Rev. D 86 (2012) 051103(R).
[15] V.M. Abazov, et al., D0 Collaboration, Precision measurement of the top quark mass in lepton + jets final states, Phys. Rev. Lett. 113 (2014) 032002;
V.M. Abazov, et al., D0 Collaboration, Precision measurement of the top-quark mass in lepton + jets final states, Phys. Rev. D 91 (2015) 112003.
[16] V.M. Abazov, et al., D0 Collaboration, Precise measurement of the top quark mass in the dilepton channel at D0, Phys. Rev. Lett. 107 (2011) 082004.
[17] T. Aaltonen, et al., CDF Collaboration, Top quark mass measurement using the template method at CDF, Phys. Rev. D 83 (2011) 111101.
[18] ATLAS, CDF, CMS, and D0 Collaborations, First combination of tevatron and LHC measurements of the top-quark mass, arXiv:1403.4427.
[19] T. Aaltonen, et al., CDF Collaboration, Measurement of the top-quark mass in the $t\bar{t}$ dilepton channel using the full CDF run II data set, arXiv:1505.00500.
[20] G. Aad, et al., ATLAS Collaboration, Measurement of the top quark mass in the $t\bar{t} \to lepton + jets$ and $t\bar{t} \to dilepton$ channels using $\sqrt{s} = 7$ TeV ATLAS data, arXiv:1503.05427.
[21] S. Chatrchyan, et al., CMS Collaboration, Measurement of the top-quark mass in $t\bar{t}$ events with dilepton final states in pp collisions at $\sqrt{s} = 7$ TeV, Eur. Phys. J. C 72 (2012) 2202.
[22] V.M. Abazov, et al., D0 Collaboration, The upgraded D0 detector, Nucl. Instrum. Methods A 565 (2006) 463.
[23] R. Angstadt, et al., The layer 0 inner silicon detector of the D0 experiment, Nucl. Instrum. Methods A 622 (2010) 298.
[24] The pseudorapidity is defined as $\eta = -\ln[\tan(\theta/2)]$ where θ is the polar angle relative to the proton beam direction
[25] V.M. Abazov, et al., D0 Collaboration, Electron and photon identification in the D0 experiment, Nucl. Instrum. Methods A 750 (2014) 78.
[26] V.M. Abazov, et al., D0 Collaboration, Muon reconstruction and identification with the run II D0 detector, Nucl. Instrum. Methods A 737 (2014) 281.
[27] G. Blazey, et al., Run II jet physics: proceedings of the run II QCD and weak boson physics workshop, arXiv:hep-ex/0005012, 2000.
[28] V.M. Abazov, et al., D0 Collaboration, Improved b quark jet identification at the D0 experiment, Nucl. Instrum. Methods A 763 (2014) 290.
[29] V.M. Abazov, et al., D0 Collaboration, Measurement of the asymmetry in angular distributions of leptons produced in dilepton $t\bar{t}$ final states in $p\bar{p}$ collisions at $\sqrt{s} = 1.96$ TeV, Phys. Rev. D 88 (2013) 112002.
[30] V.M. Abazov, et al., D0 Collaboration, Jet energy scale determination in the D0 experiment, Nucl. Instrum. Methods A 763 (2014) 442.
[31] M. Mangano, et al., ALPGEN, a generator for hard multiparton processes in hadronic collisions, J. High Energy Phys. 07 (2003) 001;
M. Mangano, M. Moretti, R. Pittau, Multijet matrix elements and shower evolution in hadronic collisions: $Wb\bar{b} + n$ jets as a case study, Nucl. Phys. B 632 (2002) 343;
F. Caravaglios, et al., A new approach to multijet calculations in hadron collisions, Nucl. Phys. B 539 (1999) 215.

[32] T. Sjöstrand, et al., High-energy-physics event generation with PYTHIA 6.1, Comput. Phys. Commun. 135 (2001) 238.
[33] M. Czakon, A. Mitov, Top++: a program for the calculation of the top-pair cross-section at hadron colliders, Comput. Phys. Commun. 185 (2014) 2930;
M. Cacciari, et al., Top-pair production at hadron colliders with next-to-next-to-leading logarithmic soft-gluon resummation, Phys. Lett. B 710 (2012) 612;
P. Baernreuther, M. Czakon, A. Mitov, Percent-level-precision physics at the tevatron: next-to-next-to-leading order QCD corrections to $q\bar{q} \to t\bar{t} + X$, Phys. Rev. Lett. 109 (2012) 132001.
[34] R. Brun, F. Carminati, CERN program library long writeup W5013, 1993 (unpublished).
[35] S. Abachi, et al., D0 Collaboration, Measurement of the top quark mass using dilepton events, Phys. Rev. Lett. 80 (1998) 2063.
[36] V.M. Abazov, et al., D0 Collaboration, Measurement of the top quark mass in final states with two leptons, Phys. Rev. D 80 (2009) 092006.
[37] M.G. Bowler, e^+e^- production of heavy quarks in the string model, Z. Phys. C 11 (1981) 169.
[38] Y. Peters, K. Hamacher, D. Wicke, Precise Tuning of the b Fragmentation for the D0 Monte Carlo, FERMILAB-TM-2425-E, 2006.
[39] S. Frixione, et al., Single-top hadroproduction in association with a W boson, J. High Energy Phys. 07 (2008) 029;
S. Frixione, et al., Single-top production in MC@NLO, J. High Energy Phys. 03 (2006) 092;
S. Frixione, B. Webber, Matching NLO QCD computations and parton shower simulations, J. High Energy Phys. 06 (2002) 029.
[40] G. Corcella, et al., HERWIG 6: an event generator for hadron emission reactions with interfering gluons (including supersymmetric processes), J. High Energy Phys. 01 (2001) 010.
[41] P. Skands, Tuning Monte Carlo generators: the Perugia tunes, Phys. Rev. D 82 (2010) 074018;
P. Skands, Tuning Monte Carlo generators: the Perugia tunes, arXiv:1005.3457, 2011.
[42] J. Pumplin, et al., New generation of parton distributions with uncertainties from global QCD analysis, J. High Energy Phys. 07 (2002) 012.